Catalysis Today 171 (2011) 140–149

Contents lists available at ScienceDirect

Catalysis Today

journal homepage: www.elsevier.com/locate/cattod

Dry reforming of methane over Pt/PrCeZrO catalyst: Kinetic and mechanistic features by transient studies and their modeling

V.A. Sadykov[a,b,*], E.L. Gubanova[a], N.N. Sazonova[a], S.A. Pokrovskaya[a,b], N.A. Chumakova[a,b], N.V. Mezentseva[a], A.S. Bobin[a], R.V. Gulyaev[a], A.V. Ishchenko[a], T.A. Krieger[a], C. Mirodatos[c]

[a] Boreskov Institute of Catalysis SB RAS, 630090 Novosibirsk, Russia
[b] Novosibirsk State University, 630090 Novosibirsk, Russia
[c] Institut de Recherches sur la catalyse et l'environnement de Lyon, Lyon, France

ARTICLE INFO

Article history:
Received 31 October 2010
Received in revised form 29 March 2011
Accepted 1 April 2011
Available online 5 May 2011

Keywords:
Methane dry reforming
Pt
Fluorite-like oxides
Transient studies
Kinetics
Mechanism
Modeling

ABSTRACT

The effect of pretreatment and Pt content on the catalytic properties as well as mechanistic features of DR were investigated for structured catalysts comprised of Pt supported on CeO_2–ZrO_2 oxide doped by Pr. Progressive reduction of cationic Pt species by the reaction feed lowers the activity in CH_4 dry reforming while accelerating the reverse water gas shift reaction catalyzed only by Pt^0, which then decreases progressively the H_2/CO ratio in the effluent. This process is counteracted by the mobility of surface oxygen supplying oxygen atoms to reduced Pt centers thus ensuring their reoxidation and generating in parallel surface oxygen vacancies for the dissociation of CO_2.

A mathematical model and software were developed for numerically studying the transients of the complex catalytic reactions. The processing of experimental data was fulfilled taking into account the importance of cationic forms of Pt, reactivity of carbonate complexes coordinated to these cations and oxygen surface/bulk diffusion. A quantitative evaluation of the density of catalyst's active sites and their coverage by reactive species was accomplished and the rates both of the lattice oxygen diffusion and main stages of the catalytic reaction were estimated.

1. Introduction

Reforming of CH_4 with CO_2 is an attractive reaction due to the production of syngas with a low H_2/CO ratio, suitable for oxo- and Fischer–Tropsch synthesis processes [1,2]. Moreover, methane dry reforming (DR) offers the additional advantage of consuming two greenhouse gases, transforming them into products with high added value. The reaction is also suitable for chemical energy transmission systems [3]. However, the commercial application of dry reforming reaction is limited due to the lack of effective catalysts resistant to carbon formation.

Most group VIII metals, especially Ni based and noble metals have been studied as catalysts for steam reforming, dry reforming, partial oxidation and mixed reforming of methane [4–8]. The deactivation is the main problem to tackle for design of a catalyst suitable for an industrial application. The two most prominent causes for the deactivation in DR are coke deposition and sintering of the active metal phase. Most of the researchers agree that coke formation is the main cause of deactivation. Carbon deposition results from two reactions, methane decomposition ($CH_4 \rightarrow C + 2H_2$) and/or Boudouard reaction ($2CO \rightarrow C + CO_2$). The type and the nature of the formed coke depend on the active metal and in many cases on the support used. In the recent literature reports ceria and zirconia materials have attracted attention as carrier or catalysts for important industrial or environmentally friendly reactions. In addition, the use of ceria-based oxides is known to prevent an accumulation of carbon on the surface of the catalysts thus helping to maintain the activity [9–12]. Literature data demonstrate that CeO_2-based oxides remarkably modify the activity of supported metals [13,14]. $Pt/Ce_xZr_{1-x}O_2$ catalysts with a Ce/Zr ratio of 1, which have the highest redox capacity, were shown to be very active and stable in methane to synthesis gas transformation reactions [15]. However, in high-temperature (especially, hydrothermal) conditions mixed ceria–zirconia oxides are decomposed into phases enriched by ceria and zirconia, respectively, which is accompanied by sintering of both oxide substrate and supported Pt [16]. To increase thermal stability of these catalysts, ceria–zirconia is doped by rare-earth cations, Al, etc. [16,17]. Among lanthanides, Pr as dopant was shown to provide the best activity of Pt-supported ceria–zirconia catalysts in CH_4 dry reforming in concentrated feeds, which was explained by a high surface and lattice oxygen mobility required to suppress coking [18,19].

* Corresponding author at: Boreskov Institute of Catalysis SB RAS, prosp. Akad. Lavrentieva, 5, 630090 Novosibirsk, Russia. Tel.: +7 3833308763; fax: +7 3833308056.
E-mail address: sadykov@catalysis.ru (V.A. Sadykov).

0920-5861/$ – see front matter © 2011 Elsevier B.V. All rights reserved.
doi:10.1016/j.cattod.2011.04.004

Furthermore, it is also important to analyze the mechanistic pathways of the reforming reaction for developing an efficient catalyst. Different steps in the mechanism have been established for the formation of CO and H_2 from CH_4. Bradford and Vannice [20] studied the kinetics of CO_2 dry reforming over supported Pt catalysts suggesting that CH_4 is reversibly activated on Pt producing CH_x species and H_2. They also proposed that CO_2 participates in the reaction via the reverse water-gas shift (RWGS) reaction yielding OH groups which then react with adsorbed CH_x intermediates to form formate-type species (CH_xO). Those intermediates decompose then irreversibly into CO and H_2. In contrast, Wei and Iglesia argued that CH_4 dissociation is the rate-limiting step, and C atoms are the most abundant reaction intermediate on the surface, while other steps are equilibrated [21]. Another reaction scheme for the dry reforming over Pt/Al_2O_3 catalyst was proposed by O'Connor et al. [2]: the CH_4 activation proceeds on free Pt sites, and CO_2 activation is assumed to be the slowest step assisted by hydrogen to form adsorbed CO and OH. The hydroxyl groups of the alumina support are supposed to participate in the reaction mechanism. For Pt/ZrO_2 participation in the reaction mechanism of hydroxocarbonates and formates stabilized on support was suggested [2]. Maestri et al. performed a microkinetic analysis of the dry and steam reforming [22] reporting that CH_4 consumption proceeds via pyrolysis, and oxidation of formed carbon involves superficial OH groups, while CO_2 is activated via interaction with adsorbed H.

The aim of the current investigations was to elucidate the factors controlling performance of Pt-supported $Pr_{0.3}Ce_{0.35}Zr_{0.35}O_{2-x}$ catalysts in CH_4 DR at short contact times. Detailed experimental studies and modeling of the behavior of structured Pt-supported catalysts in this reaction are reported. The steady state and transient operation were studied in a tubular reactor with one-channel catalytic fragment corresponding completely to a real honeycomb monolith catalyst, which allows in turn defining the intrinsic catalytic properties at contact times of 4–5 ms. The application of this kind of structure fragment allows, due to the small amount of applied catalyst, to minimize and control the temperature gradients along the channel [19,23]. The computational analysis of transient experiments on the basis of original software was aimed at determining the rates of main stages of reaction mechanism and lattice oxygen diffusion.

2. Experimental

2.1. Catalysts preparation and characterization

Complex fluorite-like $Pr_{0.3}Ce_{0.35}Zr_{0.35}O_{2-x}$ oxide was prepared by a polymerized complex precursor route (Pechini) followed by drying and calcinations in air at 900 °C for 2 h as described elsewhere [17,24]. Pt (0.5, 1.6 and 4.9 wt.%) was supported from H_2PtCl_6 solution by incipient wetness impregnation followed by drying and calcination at 900 °C. The specific surface area of samples was determined from the Ar thermal desorption data by using the BET method. XRD patterns were obtained with an ARL XTRA diffractometer using Cu Kα monochromatic radiation (λ = 1.5418 Å); the 2θ-scanning region was 20–85°. The TEM micrographs were obtained with a JEM-2010 instrument (lattice resolution 1.4 Å) and acceleration voltage 200 kV. Local elemental analysis was performed with EDX method (a Phoenix Spectrometer) XPS spectra were acquired using an ES-300 spectrometer (Kratos Analytical, UK) equipped with two anodes (AlKα, 1486.6 eV and MgKα, 1253.6 eV) operated at 65 W to prevent reduction of Ce^{4+} in the surface layer. Samples were fixed on a holder by double-side scotch tape. Calibration of XP spectra were made relatively E_B(Ce3d) = 916.7 eV.

To prepare structured catalysts, triangular channels of α-Al_2O_3 monolith (wall thickness 0.2 mm, triangle side 2.33 mm, channel length 10 mm) was washcoated with slurry of oxides with addition of peptizers and surfactants and calcined at 900 °C. Pt (1.6 wt.%) was supported by the wet impregnation followed by drying and calcination under air at 900 °C.

2.2. Steady state and transient experiments

Both steady state and transient experiments were carried out at atmospheric pressure using quartz reactors and flow installation equipped with GC and on-line IR absorbance, electrochemical and polarographic gas sensors for different components as described elsewhere [23,25]. In this reactor, a single channel structural catalytic element was placed [19,23]. The active component was either placed into the triangular corundum channel as 250–500 micron fraction loosely packed within it or supported as thin (~10 microns) layers on its walls. This helps to provide the plug-flow regime of this microreactor operation and minimize the temperature gradients along the channel.

CH_4 concentration in the feed was varied in the range of 3.5–7% with CH_4/CO_2 ratio = 1, the temperature range was 650–800 °C and contact time 4.7–15 ms. Before reaction, the samples were pretreated in O_2 stream at 700 °C. Effect of pretreatment in different streams (O_2, dry He at 900 °C; 1%CO in N_2 or 1%CH_4 in N_2 or pure H_2 at 500 °C for 0.5 h; pure H_2 at 800 °C for 0.5 h) has been studied as well. In the transient experiments after preconditioning a pretreatment flow was purged by He, and then He stream was switched to required reaction mixture. The composition of the mixture was continuously analyzed. Control experiments with a single channel fragment of the corundum showed that, at gas flow rates of about 30 l h^{-1}, the purge time of the system is no longer than 2–4 s.

3. Results and discussion

3.1. Catalysts characterization

For dispersed $Pr_{0.3}Ce_{0.35}Zr_{0.35}O_{2-x}$ oxide, specific surface area is 29 m^2/g. For promoted by Pt samples it varies in the range of 14.6–13.5 m^2/g decreasing with Pt content. This suggests that a part of supported Pt is encapsulated within support particles sintered due to their surface activation by acidic H_2PtCl_6 solution followed by high-temperature calcination [26]. XRD patterns correspond to fluorite-like solid solution [24,27]. In addition, for Pt-promoted samples with Pt loading 1.6 and 4.9 wt.%, reflections at 2θ ~39, 47, 68, 83° corresponding to metal Pt particles with typical sizes ~40–60 nm were observed, their intensity increasing with Pt content. As revealed by analysis of integral intensity of these reflections using Pt/corundum sample as a standard, only a small (<10%) part of Pt is present as metallic particles detected by XRD, which is a typical feature of Pt-supported doped ceria-(ceria–zirconia) oxides [24,26]. This conclusion is supported by TEM data (Figs. 1–3). For as-prepared samples (Fig. 1) only small (typical sizes up to several nanometers) Pt clusters strongly interacting with support and possibly covered by support oxidic fragments are revealed. For samples with the highest Pt content, big Pt particles are very seldom observed at the edges of support platelets. After sample contact with the reaction feed 7% CH_4 + 7% for 5 h at 800 °C, the number of Pt clusters per the support surface unit and their size appear to be somewhat increased, without any pronounced sintering (Fig. 2). Big Pt particles are much more frequently observed after strong reduction by H_2 at 800 °C, though small clusters were observed as well being apparently better crystallized than those on the surface of oxidized samples (Fig. 3).

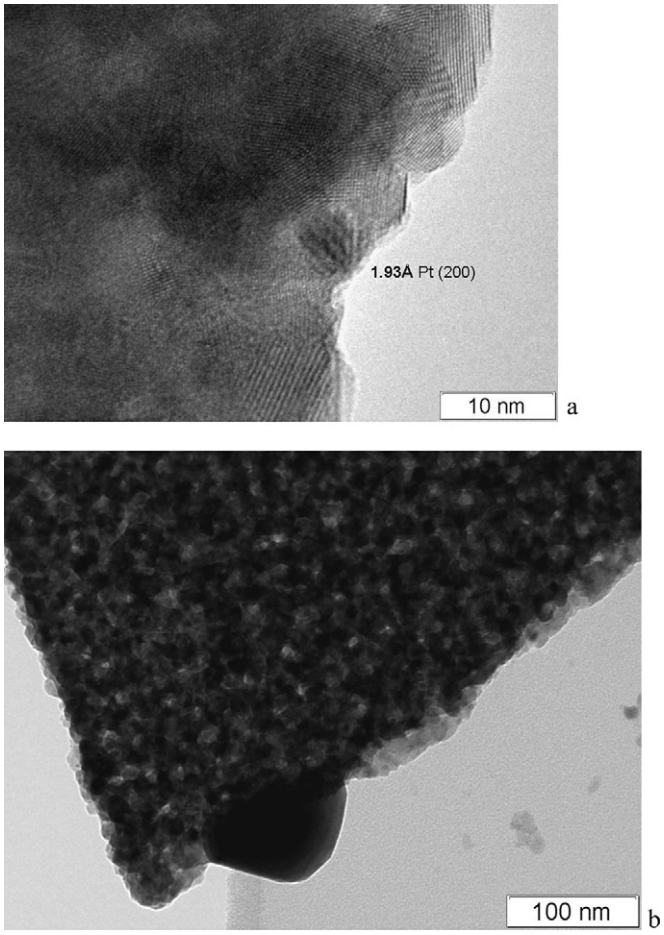

Fig. 1. Typical morphology of Pt particles in oxidized Pt/PrCeZrO samples. (a) Disordered Pt cluster on the surface of 1.6%Pt/PrCeZrO sample, (b) big Pt particle at the edge of support platelet in 4.9%Pt/PrCeZrO sample.

In general, XPS results (Fig. 4) agree with XRD and TEM data. For oxidized samples, three different states of Pt (BE 71-72, 73 and 75 eV) corresponding to species in 0, 2+ and 4+ states [28,29] have been observed (Fig. 4). For sample with the lowest Pt loading, Pt^0 state was not detected. The ratio of surface concentrations of Pt/Pr + Ce + Zr increases from ~0.2% to ~0.45% and ~1% with increasing Pt loading from 0.5 to 1.6 and 4.9 wt.%, respectively. Such a low surface concentration of Pt suggests incorporation of Pt cations into the surface/subsurface layers of fluorite-like oxides and its strong interaction with support (decoration of Pt clusters by support oxidic species) [26]. This agrees with data of infrared spectroscopy of CO test molecules adsorbed on the surface of such samples at liquid N_2 temperature revealing domination of Pt^{2+} and Pt^{+} cationic species [17,24,25]. Pt^{4+} cations even if present on the oxidized surface could not be detected by this method due to reduction by CO even at 77 K. Pretreatment of sample with 1.6% Pt in the reaction feed at high temperature results in reduction of Pt^{2+} to metallic Pt (Fig. 4) while Pt/Pr + Ce + Zr ratio only slightly decreases from ~0. 45% to ~0.4% in agreement with TEM data. High-temperature reduction of this sample by H_2 decreases further Pt/Pr + Ce + Zr ratio to ~0.2%.

3.2. Catalytic activity

3.2.1. Steady-state characteristics

Typical transients observed after contact of oxidized catalyst fraction filling the corundum channel are shown in Fig. 5 for sample with the highest Pt content. For the steady-state regime achieved at times on-stream >3000 s, the effective first-order rate constants were estimated by using the equation for the plug-flow reactor following earlier described approaches [19]. These constants varying in the range of 1–4 m^{-2} s^{-1} are roughly proportional to the surface Pt concentration estimated by XPS (vide supra). At all temperatures, H_2/CO ratio is <1 (Fig. 5), which is the usual feature of CH_4 dry reforming explained by the parallel occurrence of reverse water gas shift (RWGS) reaction consuming hydrogen

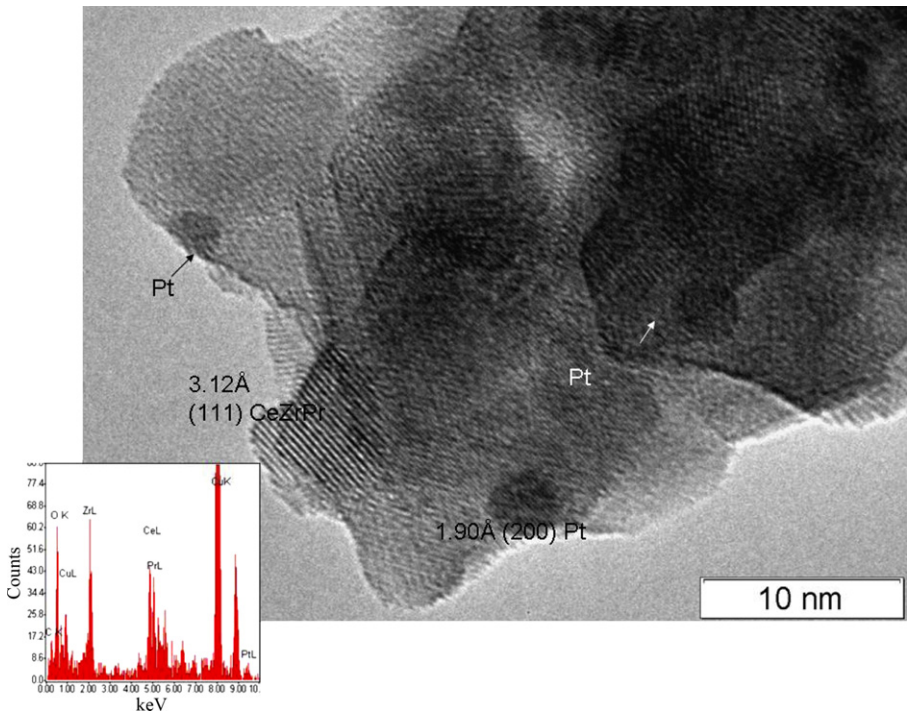

Fig. 2. Typical morphology of Pt clusters on the surface of 1.6%Pt/PrCeZrO sample treated in the reaction at high temperatures and respective EDX spectra.

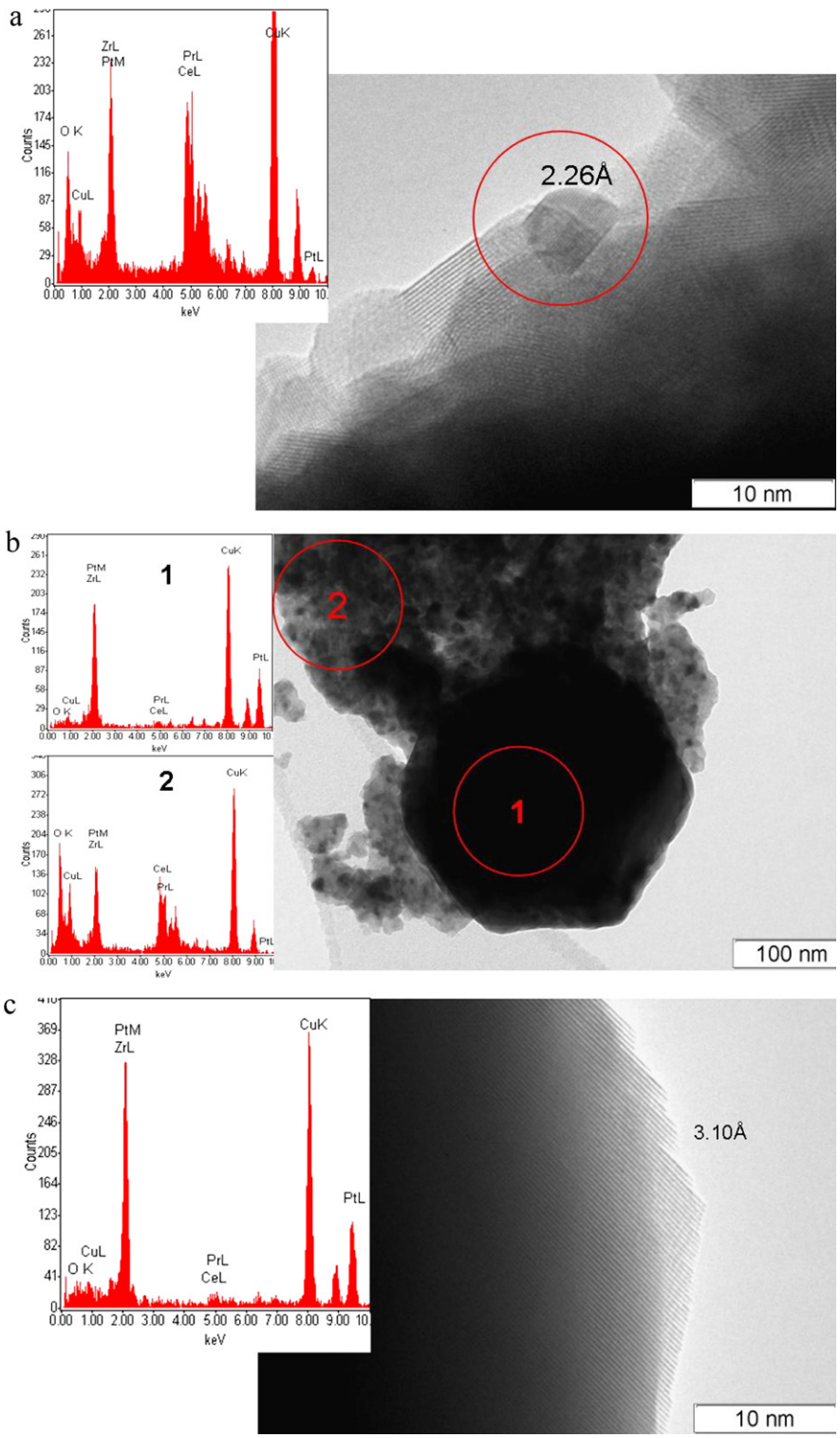

Fig. 3. Typical morphology of Pt particles on the surface of 1.6%Pt/PrCeZrO sample after reduction by H_2 at 800 °C and respective EDX spectra. (a) Small ordered Pt platelet, (b) big Pt particle, (c) high resolution image of the edge of big Pt particle.

and producing H_2O and CO [31]. Comparison of the WGS reaction product ($[H_2]^*[CO_2]$)/($[CO]^*[H_2O]$) with respective equilibrium constant calculated following known approaches [32] (Fig. 6) shows that for sample with a low Pt content this reaction is far from equilibrium. For samples with higher Pt loadings, within uncertainty of analysis, WGSR is rather close to equilibrium, though some deviation due to faster WGSR appears to take place. Hence, at a low Pt loading, RWGS reaction is hampered due to domination of oxidic Pt species not able to activate hydrogen molecules. For samples with higher Pt loadings, some deviation from the WGS reaction equilibrium can be explained either by a slow rate of direct step due to a weak bonding of CO with Pt clusters [31] or conjugation of the reverse WGS reaction with methane dry reforming as suggested by Bradford and Vannice [20]. Since slow transients observed for pretreated in O_2 Pt-supported catalysts (Fig. 5) can be caused by samples reduction in the reaction feed [19,23], special experiments

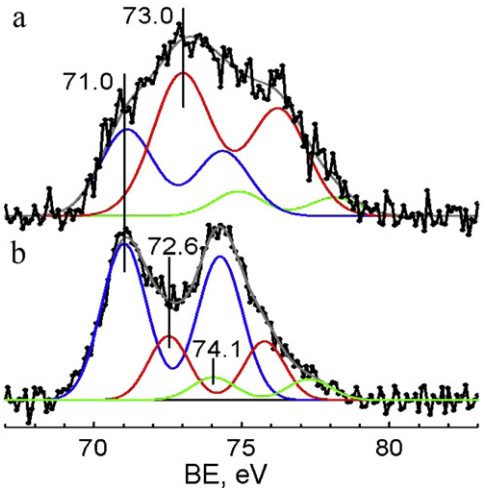

Fig. 4. XPS spectra for 1.6%Pt/PrCeZrO sample after oxidizing pretreatment (a) and after high-temperature treatment in the reaction feed 7% CH_4 + 7% CO_2 in He.

were carried out to clarify the effect of pretreatment on catalysts performance.

3.2.2. *Effect of pretreatment*

Pretreatment in H_2 at 800 °C for 0.5 h leading to complete reduction of fluorite-like oxide strongly deactivates catalysts decreasing CH_4 and CO_2 conversion from ~40–50% to ~10% at 700 °C and 15 ms. According to TEM data (Fig. 3), reduction in H_2 at 800 °C generates big Pt particles located on support, and, as judged by XPS, dispersion of Pt decreases in average as well. EDX spectrum from the edge of such a particle demonstrates that it is essentially free from any trances of Pr, Sm or Zr cations. Hence, deactivation of catalysts due to high-temperature reduction could not be assigned to any effects of strong metal –support interactions such as formation of surface PtCe alloys or ceria overlayers [26]. Rather, it can be explained not only by decreasing Pt surface area but also by ordering the structure of Pt clusters and decreasing their surface coverage by oxidic fragments. While ordering apparently decreases coordinative unsaturation of Pt, and, hence, its reactivity with respect to C–H bond activation in methane molecule [21], decreasing the surface coverage of Pt clusters by oxidic/carbonate species derived from support decreases the Pt-support interface and clearly hampers support-Pt reverse oxygen spillover. All these factors appear to be reflected in the catalyst deactivation caused by severe reduction. On the other hand, such factor as support excessive reduction could not be too important, since in the presence of CO_2 in the reaction feed support can be rapidly reoxidized by carbon dioxide to the steady-state level of stoichiometry. Reduction by H_2 at 500 °C for 0.5 h (removes up to 5 oxygen monolayers [17]) does not change the steady-state activity though transients varied significantly (not shown for brevity). Since features of transients could be affected by the radial and axial mixing occurring even within a narrow channel filled with the catalyst fraction or byproducts (CO_2, H_2O) diffusion within porous catalysts particles with typical sizes up to 0.5 mm, detailed studies of these transients as dependent upon the type of pretreatment have been carried out for thin (~10 microns) layers of 1.6 wt.% Pt/PrCeZrO catalyst supported on walls of separate corundum channel. Selection of this composition as a basic for these studies was determined by compromise between its reasonably good activity and Pt content acceptable for any practical application.

Transient curves of reagents and products responses after switching the stream of He to the reaction feed for this structured catalytic element pretreated in different conditions are presented in Fig. 7. Oxidized catalyst has the highest activity, probably due to a better activation of methane on cationic Pt species stabilized due to interaction with support [20]. For oxidized catalyst, the maximum value of H_2/CO ratio achieved up to 20–30 s of transient after switch from He to CH_4 + CO_2 stream is close to 1. This suggests that CH_4 DR on cationic Pt sites could include interaction of activated CH_x species and (hydroxo)carbonate located in the coordination sphere of the same Pt cation. The lower is the degree of oxidation varied due to pretreatment (pretreatment in He removes up to 0.5 monolayer of oxygen, pretreatment in CO or H_2 removes up to 3 monolayers), the lower is the maximum H_2/CO ratio (Fig. 7e). This shows that the reverse water-gas-shift reaction is indeed favored by the catalyst reduction. Progressive reduction of oxidized catalyst by reaction feed decreases activity in CH_4 reforming with time-on-stream while accelerating reverse water gas shift reaction catalyzed only by Pt^0, thus progressively decreasing H_2/CO ratio in products. Note that pretreatment in He leading to rather mild reduction of catalyst affects fast CO transients even stronger than reduction by CO or CH_4 (Fig. 7). Since high-temperature pretreatment in He not only removes oxygen from support and reduces Pt^{4+} cations to $Pt^{2+/1+}$ state, but also causes a pronounced dehydroxylation of the oxide as well, this suggests that, in agreement with hypothesis of Bradford and Vannice [20], hydroxyls could be involved in the reaction sequence of CH_4 dry reforming reacting with activated CH_x species at least in unsteady-state conditions. Though reduction by CH_4 not only removes the oxygen from fluorite-like oxide but also generates some coke precursors due to methane pyrolysis on Pt^0 sites [17], in studied experimental conditions transients after pretreatment by CO and CH_4 were identical. Hence, the coke precursors even if formed in these mild pretreatment conditions apparently do

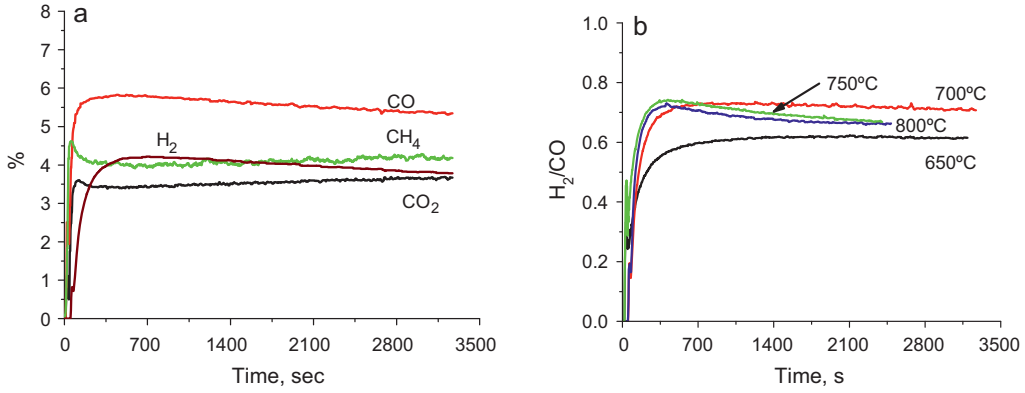

Fig. 5. Typical transients at contact of oxidized 4.9Pt/$Pr_{0.3}Ce_{0.35}Zr_{0.35}O_x$ catalyst with reaction feed at 700 °C (a) and respective variation of H_2/CO ratio in effluent with time-on-stream at different temperatures (b). 7% CH_4, CH_4/CO_2 = 1, contact time 15 ms.

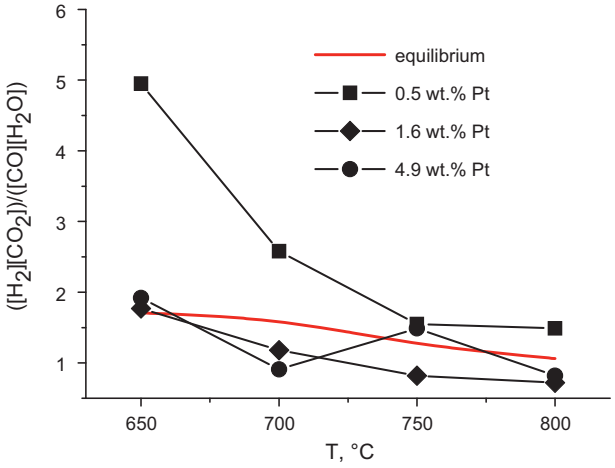

Fig. 6. Temperature dependence of reaction product for WGSR in the course of CH_4 dry reforming on Pt-supported Pr-Ce-Zr-O catalysts (points) and equilibrium constant (line).

not affect the surface steps. Note also that pretreatment by CO or CH_4 not only decreases initial conversions of reagents and concentration of products but also provides a faster deactivation of the catalyst. Hence, transfer of surface or bulk oxygen species from the oxide support to Pt/support interface apparently helps to stabilize highly active Pt cationic species. Hence, these experiments revealed that the most active and selective state of Pt/PrCeZrO catalyst is achieved after oxidizing pretreatment. So, to clarify the mechanistic aspects of CH_4 dry reforming on this catalyst, detailed transient studies have been carried out after oxidizing pretreatment of this sample with a broad variation of contact times and temperatures of experiments.

3.3. Effect of temperature and contact time on transients

Fig. 8 presents the transient data obtained at shorter contact times (higher feed rates) when the dead time effect of the system purging is minimized. These results in general agree with those obtained at lower temperatures and longer contact times (Fig. 7). Conversion of reagents, concentration of products and H_2/CO ratio

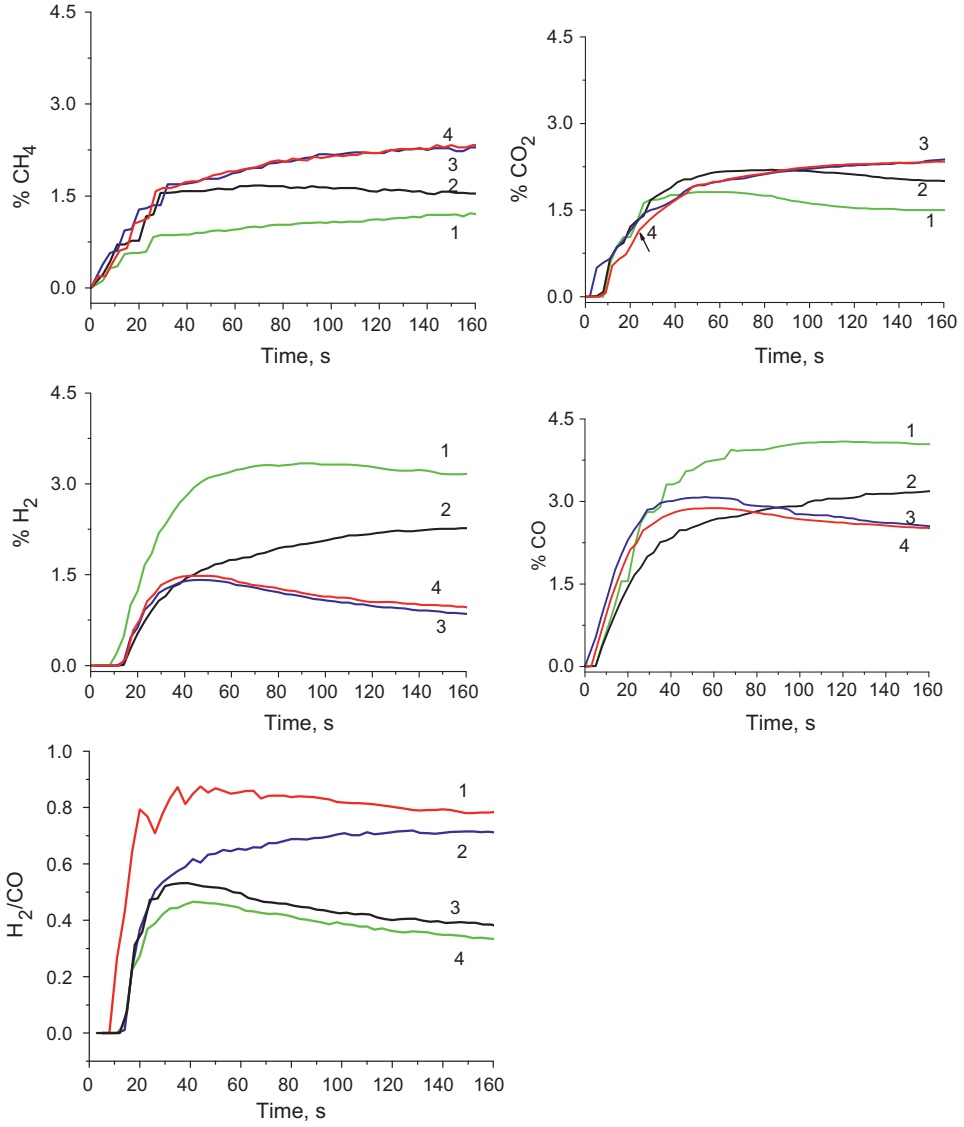

Fig. 7. Effect of pretreatment type (numbered 1–4 on curves) on reaction component transients observed for structured 1.6 wt.% $Pt/Pr_{0.3}Ce_{0.3}Zr_{0.35}O_{2-x}$ catalyst. Feed composition: 3.5% of methane at $CH_4/CO_2 = 1$, contact time 15 ms, $T = 650\,^{\circ}C$. Pretreatment conditions: 1 – pretreatment in O_2, 2 – pretreatment in He, 3 – pretreatment in 1%CO in He, 4 – pretreatment in 1% CH_4 in He; pretreatment time 60 min; temperature of pretreatment 900 °C (1, 2) or 500 °C (3, 4).

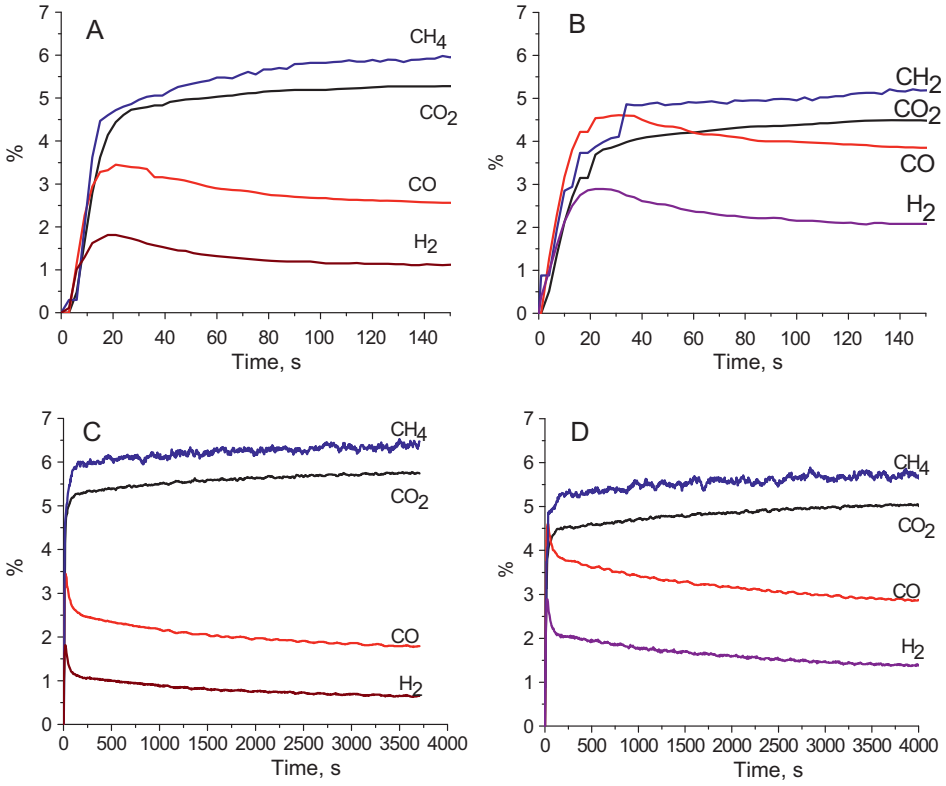

Fig. 8. Fast (A,B) and slow (C,D) parts of for oxidized structured 1.6 wt.% $Pt/Pr_{0.3}Ce_{0.3}Zr_{0.35}O_{2-x}$ catalyst after contact with feed 7% CH_4 + 7% CO_2 in He at 750 °C. Contact time 4.72 ms (A,C) and 8 ms (B,D).

increase with the contact time (Fig. 8). These transients were analyzed in details by applying mathematical modeling.

3.4. Modeling

The mathematical model and software were developed for numerical studying the transients of a complex catalytic reaction in the plug-flow reactor where a fragment with a single channel of the catalytic monolith is placed. The process model describes both the conversion of oxygen-containing species on the catalyst surface by reaction steps and the surface/near surface mobility of oxygen.

3.4.1. Kinetic scheme

The reaction scheme of methane dry reforming has been considered that includes the syngas formation by interaction of methane and CO_2 as well as the water-gas shift reaction. The rates of Boudouard reaction and CH_4 decomposition are assumed to be negligible, so coke formation in the time range considered here is not taken into account.

The analysis of experimental data given above shows that reaction steps on the catalyst surface could occur on the Pt centers as well as on the available active sites of CeO_2–ZrO_2 mixed oxide schematically presented in Fig. 9.

The kinetic scheme consisting of 6 catalytic stages has been considered. The catalytic stages have been selected on the basis of the analysis of experiments presented above as well as the literature data [2]. The scheme reflects the methane transformation on the active cationic Pt-centers, stabilization of Pt centers by the lattice oxygen, the interaction of carbon dioxide with oxidized Pt centers and surface oxygen vacancies of the catalyst layer, and the step providing RWGS reaction pathway:

$$\begin{aligned}
&1)\ CO_2 + [PtO] \leftrightarrow [PtCO_3]\\
&2)\ CH_4 + [PtCO_3] \rightarrow 2CO + 2H_2 + [PtO]\\
&3)\ CH_4 + [PtO] \rightarrow CO + 2H_2 + [Pt]\\
&4)\ [Pt] + [O_s] \leftrightarrow [PtO] + [V_s]\\
&5)\ CO_2 + [V_s] \rightarrow CO + [O_s]\\
&6)\ H_2 + [PtO] \rightarrow H_2O + [Pt]
\end{aligned} \qquad (1)$$

Here [PtO] and [Pt] denote the oxidized and vacant Pt-centers, $[PtCO_3]$ is the carbonate complex, $[O_s]$ and $[V_s]$ are the oxidized and vacant sites inside the lattice layer.

The following stoichiometric pathways correspond to this set of catalytic stages:

$$\begin{aligned}
&\text{I. } CH_4 + CO_2 \leftrightarrow 2CO + H_2\\
&\text{II. } CO_2 + H_2 \leftrightarrow CO + H_2O
\end{aligned} \qquad (2)$$

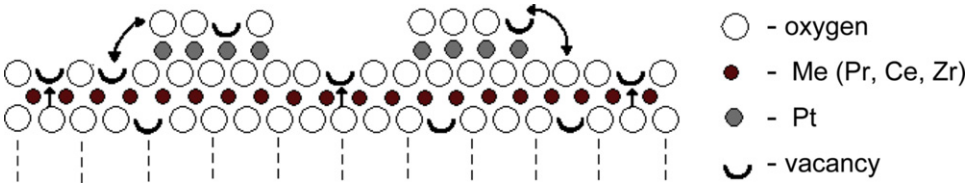

Fig. 9. Scheme of the near-surface layer of Pt/PrCeZrO catalyst.

According to the mass action law the rates of catalytic steps look as follows:

$$\begin{aligned} r_1 &= k_1 C_{CO_2}\theta_1, \qquad r_{-1} = k_{-1}\,\theta_2 \\ r_2 &= k_2 C_{CH_4}\theta_2 \\ r_3 &= k_3 C_{CH_4}\theta_1 \\ r_4 &= k_4(1-\theta_1-\theta_2)\theta_3, \qquad r_{-4} = k_{-4}\theta_1(1-\theta_3) \\ r_5 &= k_5 C_{CO_2}(1-\theta_3) \\ r_6 &= k_6 C_{H_2}\theta_1 \end{aligned} \tag{3}$$

where r_i is the rate of the ith catalytic stage (i = 1,2,. . ., 6); C_{CH_4}, C_{CO_2}, and C_{H_2} are the concentrations of H_4, CO_2 and H_2 in the gas mixture correspondingly; θ_1, θ_2, and θ_3 are the relative surface concentrations of oxidized Pt-centers [PtO], carbonate complexes [$PtCO_3$], and oxidized lattice layer sites [O_s] respectively; k_i is the rate constant of the ith catalytic stage (i = 1,2,. . ., 6).

It is assumed that the total number of active Pt-centers is equal to

$$[ZO] + [ZCO_3] + [Z] = \alpha N_\theta, \tag{4}$$

and the number of active lattice layer sites available for spillover is equal to

$$[ZO^*] + [Z^*] = \beta N_\theta \tag{5}$$

where N_θ is the total number of active centers on the catalyst surface, α is the relative surface concentration of Pt-centers, β is the ratio of the number of active lattice layer sites under the surface to the total number of active surface centers.

Since Pt^{4+} cations are easily transformed into Pt^{2+} even after catalyst purging by He at high temperatures after pretreatment in O_2, and reoxidation of Pt^{2+} cations to Pt^{4+} state by oxygen atoms migrating from support is apparently impossible under reaction conditions, Pt^{4+} cationic species revealed by XPS were not considered separately in suggested reaction scheme.

3.4.2. Mathematical model and numerical algorithm

The preliminary estimates of the intraparticle pore-diffusion resistance inside the catalyst fragment, the rates of axial diffusion and mass transfer between the catalyst channel wall and reacting gas mixture flow [33] showed that these processes do not influence significantly the rates of catalytic transformations. Therefore, the mathematical description includes the following equations:

- the first-order partial differential equations of the mass balance of the reagents and products in the gas phase (CO_2, CH_4, CO, and H_2) which reflect both the convective term due to the gas flow along the catalyst fragment length and the term related to the chemical transformations of the reactive mixture components on the catalyst surface at every cross-section of the channel,
- the second order parabolic type equation at each axial position describing the unsteady oxygen transport from the near surface layers of the catalyst lattice towards the active Pt-centers on the catalyst surface where the catalytic reaction proceeds (the diffusion mechanism is assumed),
- two ordinary differential equations describing the time behavior of the concentrations of oxidized Pt centers and carbonate complexes on the catalyst surface at each axial cross-section point; the dynamics depends on the local rates of catalytic transformations at the surface and of oxygen diffusion through the catalyst lattice.

Thus, the developed mathematical model is the initial-boundary value problem for a system of differential equations of different type.

The algorithm proposed bases on the second order finite-difference approximation with respect to two spatial coordinates (the length of the catalyst fragment, the distance between a point inside the catalyst lattice and the catalyst surface) and time. At each time step, the method of alternating directions is used to construct the numerical solution of the discrete approximation equations.

3.4.3. Modeling results

Using the software developed, a number of computational transient runs have been performed with the process parameters corresponded to the experimental response curves after reaction mixture feed on the catalyst pretreated in O_2 stream: gas feed rate u = 10.6 and 18 l h^{-1}, temperature T = 750 °C, inlet concentrations both of CH_4 and CO_2 are 7%, contact time τ = 4.7 and 8 ms.

It has been assumed that

(a) The total number of active centers on the catalyst surface is equal to maximal monolayer coverage $N_\theta = 1.28 \times 10^{15}$ at O/cm^2.
(b) Before reaction mixture feeding, at time t = 0, all active centers are oxidized, i.e., $\theta_1 = \theta_2 = 1$.

At first, the verification of the hypothesis about the kinetic scheme given above was carried out. For this purpose, the computational runs of transient regimes have been performed on the base of mathematical model with the simple redox kinetic scheme that includes only three steps: 3–5 of the kinetic scheme (1), the rates of the formation and conversion of carbonate intermediates and the step of RWGS reaction are assumed to be equal to zero. Modeling has revealed that this scheme does not describe the transients since in this case concentrations of CH_4 and CO_2 change contrariwise, while in the experiment they vary in parallel (Fig. 8). Hence, a route should exist providing an efficient CO_2 transformation on the oxidized surface.

Thus, modeling has been continued with overall kinetic scheme (1). The constants of catalytic stage rates and the parameters defining the rate of oxygen supply from the lattice to the surface have been varied during the computational runs:

- rate constants of catalytic steps k_1, k_{-1}, k_2, k_3, k_4, k_{-4}, k_5, and k_6;
- the coefficient D of bulk diffusion of oxygen;
- the depth H of the subsurface layer of the catalyst lattice available for oxygen mobility;
- the fraction α of the surface covered by Pt-centers;
- the fraction β of the surface with active lattice layer sites.

The initial approximation for all parameters of the model for processing has been estimated from the steady state experimental data and the data of XPS, FTIRS of adsorbed CO and oxygen isotope exchange [17,25,27,30]. Results of computations revealed that in studied conditions, the time of relaxation determined by achievement of catalyst steady state coverage by reactive species involved in catalytic cycle could not exceed few seconds, which agrees with analytic simple estimations following approach suggested by Temkin [34].

Analyzing the transient curves up to 300 s, it has been demonstrated convincingly that

- the character and shape of response curves is mainly defined by the rates of carbonates formation and consumption, the rates of "spillover," and the subsequent interaction of CO_2 with vacant centers of the catalyst oxide;
- the transient time period is determined by parameters characterizing the catalyst structure and the lattice oxygen mobility, such as the catalyst specific surface S_b, the quantity of active centers on the catalyst surface N_θ, the fractions of the surface Pt centers

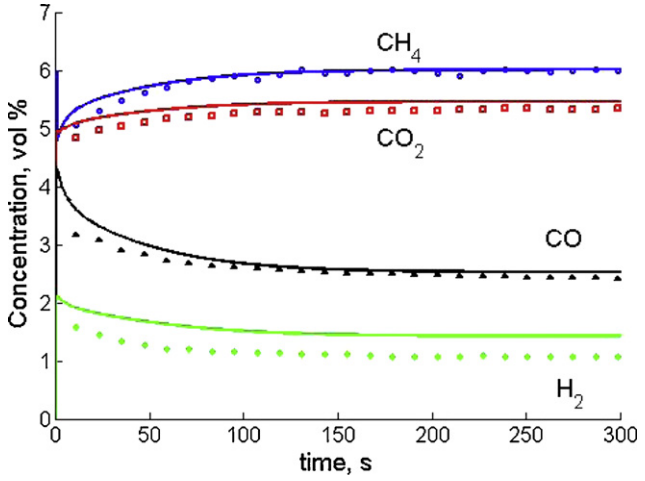

Fig. 10. Comparison of the experimental (points) and computed (lines) time dependences of concentrations in transient experiments 750 °C, gas feed rate 18 l h^{-1}, feed 7%CH_4 + 7%CO_2 in He, contact time 4.7 ms.

α and the lattice layer sites β, the rate and characteristic length of the oxygen bulk diffusion.

Data processing has allowed to evaluate the kinetic parameters and characteristics of the catalyst structure. Some examples of comparing modeling and experimental results are given in Fig. 10 for the following values of parameters: $\tau = 4.7$ s, $k_1 = 200\,s^{-1}$, $k_{-1} = 0.6\,s^{-1}$, $k_2 = 600\,s^{-1}$, $k_3 = 60\,s^{-1}$, $k_4 = 300\,s^{-1}$, $k_{-4} = 5\,s^{-1}$, $k_5 = 55\,s^{-1}$, $k_6 = 1100\,s^{-1}$, $\alpha = 0.04$, $\beta = 0.2$, $S_b = 20 \times 10^4\,cm^{-1}$, $D = 2.5 \times 10^{-13}\,cm^2/s$, $H = 5 \times 10^{-6}$ cm.

Fig. 10 demonstrates that the suggested kinetic scheme reflects the main peculiarities of the catalyst behavior rather well. The experimental values of gas concentrations and the modeling data are in a good agreement. Note that the key characteristics of the catalyst (the number of oxide surface active sites, Pt surface concentration, characteristic oxygen diffusion length) determined on the base of computational results agree with the values independently estimated by XPS, FTIRS of adsorbed CO methods, and oxygen isotope exchange data [17,18,25,27,30].

Fig. 11 shows the calculated values of relative surface concentrations of Pt centers occupied by oxygen and carbonates. After feeding the reaction mixture with CH_4 and CO_2 to the system the number of oxidized Pt sites decreases quickly because of high rates of CH_4

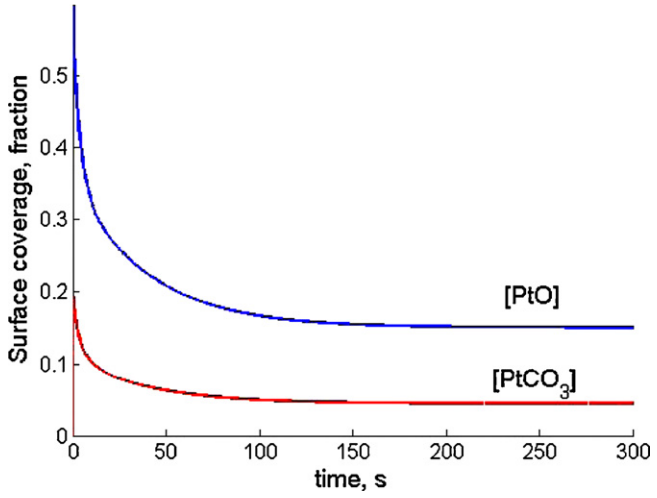

Fig. 11. Time dependence of the surface coverage fraction with intermediates [PtO] and [$PtCO_3$]. The operation conditions correspond to ones in Fig. 10.

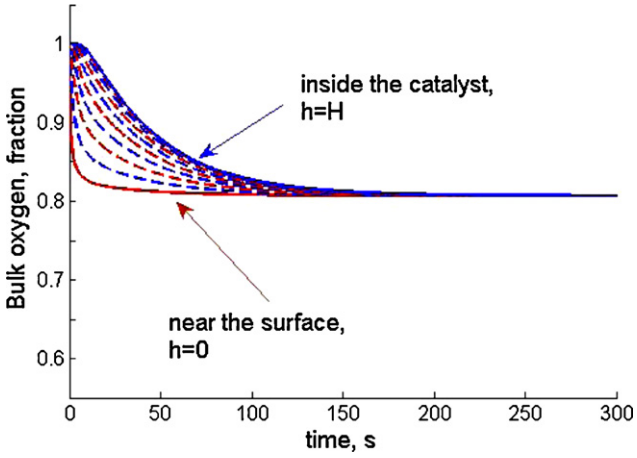

Fig. 12. Time dependence of the bulk oxygen fraction. The operation conditions correspond to ones in Fig. 10.

and CO_2 adsorption, so the surface coverage by carbonates has a sharp peak during a few seconds. Then, slow decline of these concentrations towards the steady values occurs due to stabilization of Pt centers by the oxygen of near-surface layers (Fig. 11). Similarly, concentration of bulk oxygen varies as well reaching the steady-state level within ~300 s (Fig. 12). Hence, it could be concluded that the transients caused by the catalyst reduction by reaction feed occur within ~300 s, stoichiometry of the bulk of oxide particles being affected. Longer (up to 3000 s) transients observed in our experimental conditions (Fig. 8) can be caused only by slower processes such as Pt aggregation (in general, decreasing Pt-support interface/interaction and ordering Pt clusters) and coke deposition. Since temperature-programmed oxidation by oxygen after reaction of this sample as well as TEM studies revealed no carbon deposition, Pt aggregation appears to be the main cause of slow transients. In fact, even syngas generation via route comprised of combination of steps (1) and (2) depends upon the metal-support interaction, since PtO in the absence of gas-phase oxygen can be regenerated only by oxygen migrating from the support (step 4), direct reoxidation of Pt sites by CO_2 being impossible. Apart from pure kinetic aspect, it is possible that carbonates can be stabilized only by Pt cations having as neighbors reducible cations of support such as Ce or Pr cations. Such Pt cations can be either incorporated into the surface position of support or situated at perimeter of Pt clusters. Decoration of the surface of Pt clusters by Pr or Ce oxidic species could also stabilize such carbonates coordinated to Pt cations as well.

Routes of dry reforming and RWGS corresponding to steps (3)–(6) involve also PtO sites which at present could not be reliably differentiated from those stabilizing carbonates due to lack of experimental data. So they are including in the balance of active Pt sites $[ZO] + [ZCO_3] + [Z] = \alpha N_\theta$, in Eq. (4).

Analysis of rates of CH_4 consumption by different mechanisms revealed that contribution of mechanism 1 (via carbonates) is considerably higher for the oxidized catalyst at the first seconds of contact with the reaction mixture, the ratio of step 2 and 3 rates being ~3. The decrease of the surface oxidation level results in lowering the fraction of Pt centers occupied by carbonates, and, as the result, the ratio of step rates 2 and 3 decreases to 1.6.

4. Conclusion

The combination of the steady state and transient experiments for CH_4 DR on structured Pt/PrCeZrO catalyst at millisecond contact times along with their modeling allowed to elucidate main factors responsible for the catalyst activity and performance stability. Both Pt-support interaction and lattice oxygen mobility in

the complex oxide support are responsible for the efficient performance of catalyst pretreated in O_2. Kinetic parameters of the reaction steps occurring on these catalysts were determined by processing the kinetic transients with a due regard for the oxygen species diffusion, participation of carbonate complexes stabilized in the coordination sphere of Pt cationic forms in CH_4 oxidative transformation and occurrence of reverse water gas shift reaction catalyzed by metallic Pt. Long (>3000 s) transients can be explained only by slow Pt aggregation and ordering of Pt clusters caused by complex oxide support reduction thus decreasing metal-support interaction.

Acknowledgements

This work was carried out in frames of Associated Russian–French Laboratory on Catalysis. Support by FP7 Project OCMOL, Interdisciplinary Integration Project no.107 of Siberian Branch of the Russian Academy of Sciences, RFBR–CNRS 09-03-93112 Project and Russian Federal Innovation Agency via the program "Scientific and Educational cadres" is gratefully acknowledged. The Embassy of France in Moscow is gratefully acknowledged for the joint PhD studentship grant of A. Bobin.

References

[1] F. Pompeo, N.N. Nichio, M.M.V.M. Souza, D.V. Cesar, O.A. Ferretti, M. Schmal, Appl. Catal. A 316 (2007) 175.
[2] A.M. O'Connor, Y. Schuurman, J.R.H. Ross, C. Mirodatos, Catal. Today 115 (2006) 191.
[3] J.T. Richardson, S.A. Paripatyadar, Appl. Catal. 61 (1990) 293.
[4] E. Ruckenstein, Y. Hang Hu, Appl. Catal. A 133 (1995) 149.
[5] J.R. Rostrup-Nielsen, L.J. Christiansen, Appl. Catal. A 126 (1995) 381.
[6] T. Osaki, T. Mori, J. Catal. 204 (2001) 89.
[7] S. Wang, G.Q. Lu, Appl. Catal. B 19 (1998) 267.
[8] J.M. Wei, B.Q. Xu, J.L. Li, Z.X. Cheng, Q.M. Zhu, Appl. Catal. A 196 (2000) L167.
[9] F.B. Norohna, E.C. Fendley, R.R. Soares, W.E. Alvarez, D.E. Resasco, Chem. Eng. J. 82 (2001) 21.
[10] Y. Denkwitz, A. Karpenko, V. Pizak, R. Leppelt, B. Schumacher, R.J. Behm, J. Catal. 246 (2007) 74.
[11] A. Pintar, J. Batista, S. Hocever, J. Colloid Interface Sci. 307 (2007) 145.
[12] L.F. Liotta, G. Di Carlo, G. Pantaleo, G. Deganello, Appl. Catal. B: Environ. 70 (2007) 314.
[13] J. Kašpar, P. Fornasiero, M. Graziani, Catal. Today 50 (1999) 285.
[14] S. Damyanova, B. Pawelec, K. Arishtirova, M.V. Martinez Huerta, J.L.G. Fierro, Appl. Catal. B: Environ. 89 (2009) 149.
[15] F.B. Passos, E.R. Oliveira, L.V. Mattos, F.B. Noronha, Catal. Today 101 (2005) 23.
[16] J. Kašpar, P. Fornasiero, in: A. Trovarelli (Ed.), Catalysis by Ceria and Related Materials, Imperial College Press, 2002, pp. 217–241.
[17] V.A. Sadykov, N.V. Mezentseva, G.M. Alikina, A.I. Lukashevich, Yu.V. Borchert, T.G. Kuznetsova, V.P. Ivanov, S.N. Trukhan, E.A. Paukshtis, V.S. Muzykantov, V.L. Kuznetsov, V.A. Rogov, J. Ross, E. Kemnitz, C. Mirodatos, Solid State Phenom. 128 (2007) 239.
[18] V. Sadykov, V. Muzykantov, A. Bobin, N. Mezentseva, G. Alikina, N. Sazonova, E. Sadovskaya, L. Gubanova, A. Lukashevich, C. Mirodatos, Catal. Today 157 (2010) 55.
[19] N.N. Sazonova, V.A. Sadykov, A.S. Bobin, S.A. Pokrovskaya, E.L. Gubanova, C. Mirodatos, React. Kinet. Catal. Lett. 98 (2009) 35.
[20] M.C.J. Bradford, M.A. Vannice, Appl. Catal. A: Gen. 142 (1996) 97.
[21] J. Wei, E. Iglesia, J. Catal. 224 (2004) 370.
[22] M. Maestri, D.G. Vlachos, A. Beretta, G. Groppi, E. Tronconi, J. Catal. 259 (2008) 211.
[23] E.L. Gubanova, A. Van Veen, C. Mirodatos, V.A. Sadykov, N.N. Sazonova, Russ. J. Gen. Chem. 78 (2008) 2191.
[24] V.A. Sadykov, T.G. Kuznetsova, G.M. Alikina, Yu.V. Frolova, A.I. Lukashevich, V.S. Muzykantov, V.A. Rogov, L.Ch. Batuev, V.V. Kriventsov, D.I. Kochubei, E.M. Moroz, D.A. Zyuzin, E.A. Paukshtis, E.B. Burgina, S.N. Trukhan, V.P. Ivanov, L.G. Pinaeva, Yu.A. Ivanova, V.G. Kostrovskii, S. Neophytides, E. Kemnitz, K. Scheurel, C. Mirodatos, in: D.K. McReynolds (Ed.), New Topics in Catalysis Research, Nova Science Publishers, NY, USA, 2007, pp. 97–196, Chapter 5.
[25] V. Sadykov, T. Kuznetsova, Yu. Frolova-Borchert, G. Alikina, A. Lukashevich, V. Rogov, V. Muzykantov, L. Pinaeva, E. Sadovskaya, Yu. Ivanova, E. Paukshtis, N. Mezentseva, L. Batuev, V. Parmon, S. Neophytides, E. Kemnitz, K. Scheurell, C. Mirodatos, A. van Veen, Catal. Today 117 (2006) 475.
[26] S. Bernal, J.J. Calvino, J.M. Gatica, C.L. Cartes, J.M. Pintado, in: A. Trovarelli (Ed.), Catalysis by Ceria and Related Materials, Imperial College Press, 2002, pp. 85–168.
[27] V. Sadykov, N. Mezentseva, V. Muzykantov, D. Efremov, E. Gubanova, N. Sazonova, A. Bobin, E. Paukshtis, A. Ishchenko, V. Voronin, J. Ross, C. Mirodatos, A. van Veen, Mater. Res. Soc. Symp. Proc. 1122 (2009) 1–6, 1122-O05-03.
[28] W. Yang, Y. Ma, J. Tang, X. Yang, Colloids Interface A: Phys Eng. Aspects 302 (2007) 628.
[29] Z. Yi, W. Wei, S. Lee, G. Jianhna, Catal. Commun. 8 (2007) 906.
[30] V. Sadykov, N. Mezentseva, G. Alikina, A. Lukashevich, V. Muzykantov, T. Kuznetsova, L. Batuev, M. Fedotov, E. Moroz, D. Zyuzin, V. Kolko, V. Kriventsov, V. Ivanov, A. Boronin, E. Pazhetnov, V. Zaikovskii, A. Ishchenko, V. Rogov, J. Ross, E. Kemnitz, Mater. Res. Soc. Symp. Proc. 988 (2007) 1–6, QQ06-04.
[31] N. Laosiripojana, S. Assabumrungrat, Appl. Catal. B: Environ. 60 (2005) 107.
[32] D. Wolf, M. Barré-Chassonnery, M. Höhenberger, A. van Veen, M. Baerns, Catal. Today 40 (1998) 147.
[33] N.N. Sazonova, S.N. Pavlova, S.A. Pokrovskaya, N.A. Chumakova, V.A. Sadykov, Chem. Eng. J. 154 (2009) 17.
[34] M.I. Temkin, Kinet. Catal. 17 (1976) 1095.